

Magnetocrystalline Anisotropy Energy of Transition Metal Thin Films: A Non-perturbative Theory

A. Lessard, T. H. Moos, and W. Hübner

Institute for Theoretical Physics, Freie Universität Berlin, Arnimallee 14, D-14195 Berlin, Germany
(July 16, 2018)

The magnetocrystalline anisotropy energy E_{anis} of free-standing monolayers and thin films of Fe and Ni is determined using two different semi-empirical schemes. Within a *tight-binding calculation* for the 3d bands alone, we analyze in detail the relation between bandstructure and E_{anis} , treating spin-orbit coupling (SOC) non-perturbatively. We find important contributions to E_{anis} due to the lifting of band degeneracies near the Fermi level by SOC. The important role of degeneracies is supported by the calculation of the electron temperature dependence of the magnetocrystalline anisotropy energy, which decreases with the temperature increasing on a scale of several hundred K. In general, E_{anis} scales with the square of the SOC constant λ_{so} . Including 4s bands and *s-d* hybridization, the *combined interpolation scheme* yields anisotropy energies that quantitatively agree well with experiments for Fe and Ni monolayers on Cu(001). Finally, the anisotropy energy is calculated for systems of up to 14 layers. Even after including *s*-bands and for multilayers, the importance of degeneracies persists. Considering a fixed fct-Fe structure, we find a reorientation of the magnetization from perpendicular to in-plane at about 4 layers. For Ni, we find the correct in-plane easy-axis for the monolayer. However, since the anisotropy energy remains nearly constant, we do not find the experimentally observed reorientation.

PACS: 75.30.Gw, 75.70.Ak, 75.70.-i, 73.20.Dx.

I. INTRODUCTION

The dependence of the total energy of a ferromagnetic crystal on the direction of magnetization originates from the magnetic dipole-dipole interaction as well as from spin-orbit coupling (SOC), as proposed by van Vleck¹. The magnetic anisotropy energy is expected to be enlarged in systems of low symmetry, i.e. at surfaces, interfaces, and thin films² or in one-dimensional systems such as quantum corrals³. Recently, a magnetization easy-axis perpendicular to the film plane has been observed for a wide variety of thin film systems, for example for thin films of fcc Fe on Cu(001)⁴⁻⁶. Some of these systems are promising candidates for magnetic high-density storage media.

In spite of many theoretical attempts⁷⁻¹⁵, the relation between the electronic structure and magnetocrystalline anisotropy energy E_{anis} could not be fully clarified so far. Some very important questions are subject to intense discussion: (i) Which bandstructure details lead to significant contributions to E_{anis} ? Especially the treatment of degenerate bands near the Fermi level has brought up controversies¹¹⁻¹³. (ii) How does E_{anis} depend on the SOC strength λ_{so} ? (iii) How is it influenced by the substrate lattice constant? Moreover, there is no unified thermodynamic and electronic theory to determine the temperature dependence of E_{anis} . Finally, the correct prediction of magnetic anisotropy for real systems still remains a challenge, since due to the quenching of orbital angular momentum in 3d transition metal systems, E_{anis} is several orders of magnitude smaller than other contributions to the total energy of a crystal (typically about 0.1 – 1 meV per atom in ultrathin films).

The magnetic anisotropy of thin films has been in-

vestigated using two essentially different approaches. In semiempirical calculations^{7,8,10,14}, the magnetocrystalline anisotropy energy E_{anis} is determined by means of parametrized tight-binding bandstructures. Usually, spin-orbit coupling is restricted to second order perturbation theory. On the other hand, *ab-initio* calculations have been made^{9,12,13,15} and lead to realistic bandstructures. All calculations make use of the controversial force theorem¹⁶. Convergence, however, is difficult to achieve; sometimes, additional assumptions are made in order to obtain converged results (*state tracking method*¹²).

The structure of thin Fe films deposited on Cu(001) has been widely investigated, especially the dependence of the structure and magnetization orientation on the temperature. For films of less than 5 monolayers (ML) deposited at low temperatures, a distorted fcc-structure is found, with magnetization perpendicular to the film plane. At 5 ML, a transition to in-plane magnetization is observed, as well as a restructuration of the film. It is still not clear if this reorientation transition is an effect of the structural changes taking place in the film at 4-5 ML^{5,17-20}.

In this paper, we investigate a simple quadratic Fe and Ni monolayer and fcc multilayers systems up to 14 ML epitaxially grown on the Cu(001) surface and neglect further interactions with the substrate. The bandstructures are calculated within two different semi-empirical schemes, including SOC completely non-perturbatively without resorting to degenerate or non-degenerate perturbation theory of any order. A *tight-binding calculation* of the 3d-bands allows for a detailed, **k**-space resolved analysis of the role of degeneracies for E_{anis} . It is shown that degeneracies located near the Fermi level can yield significant contributions, if they occur along *lines*

in \mathbf{k} -space. We find for these that generally $E_{anis} \propto \lambda_{so}^2$ holds. Including 4s-bands by means of the *combined interpolation scheme*²¹ and fitting the parameters to *ab-initio* calculations, we obtain the correct sign and values of E_{anis} for the systems considered with this fully convergent method. That could be achieved neither by a fit using bulk parameters nor by employing a real-space density of states calculation, the so-called recursion method¹¹. Moreover, we find the characteristic scale for the temperature dependence of the magnetic anisotropy to be λ_{so} , rather than the bandwidth. This supports the significance of the lifting of degeneracies at E_F by λ_{so} and demonstrates the importance of contributions to magnetic anisotropy due to Fermi-edge smearing.

Finally, we calculate the anisotropy energy of multi-layer systems. For systems of tetragonally-distorted Fe of 2 to 14 ML, we find a transition from magnetization perpendicular to the plane to in-plane magnetization at about 4 ML. We conclude from our calculation that the experimentally observed reorientation at 5 layers is not necessarily caused by a structural phase transition. For Ni, we find a nearly constant anisotropy energy from the fourth layer on, in disagreement with the results of Schulz and Baberschke²², who find a reorientation from in-plane to parallel magnetization at 7 ML. In both cases, the degeneracies near the Fermi-level are found to play an important role for the dependence of the anisotropy energy on the film thickness.

This paper is organized as follows: In Section II, the interpolation schemes (II.A, II.B, II.C) and the determination of E_{anis} (II.D) are presented. The results for the tight-binding scheme for d -bands alone are shown in section III.A, the role of degeneracies is analyzed in detail in III.B while the results for the complete s - and d -band calculation for Fe and Ni monolayers on Cu(001) and other substrates are given in section III.C. The influence of crystal field splitting is investigated. Some aspects of the temperature dependence of magnetic anisotropy are considered in III.D, and the results for multilayer systems are presented in III.E and III.F. Section IV sums up the most important results.

II. THEORY

A. Bandstructures

The magnetocrystalline anisotropy energy E_{anis} depends sensitively on the electronic structure of the system. To simplify the analysis, the bandstructure of the monolayer is calculated in two steps. First, the 3d-bands are described within a tight-binding scheme. Although the resulting E_{anis} as a function of the 3d-bandfilling n_d shows already the most important features, the 4s-bands and s - d -hybridization have to be taken into account for a correct numerical evaluation of E_{anis} .

For the 3d-bands, the tight-binding formalism introduced by Fletcher²³ and Slater and Koster²⁴ is adapted to the monolayer. The Hamiltonian $H^d = H_{at} + \Delta U$ is set up as a 10×10 matrix with respect to the basis of Bloch wave functions

$$\psi_{n\mathbf{k}}(\mathbf{r}) = \frac{1}{\sqrt{N}} \sum_{\mathbf{R}} e^{i\mathbf{k} \cdot \mathbf{R}} \phi_n(\mathbf{r} - \mathbf{R}). \quad (1)$$

Here, H_{at} is the atomic Hamiltonian, ΔU the additional crystal field in the monolayer. ϕ_i , $i = 1, \dots, 5$ ($i = 6, \dots, 10$) are the atomic 3d orbitals commonly denoted by xy , yz , zx , $x^2 - y^2$ and $3z^2 - r^2$ respectively, together with the spin eigenstate $|\uparrow\rangle$ ($|\downarrow\rangle$) with respect to the spin quantization axis z_M . In the simple quadratic monolayer, only orbitals located on neighboring atoms are included. The extension to second nearest neighbors does not lead to further insight²⁵. With the x - and y -axes oriented along axes connecting nearest neighbors in the monolayer, the spin-polarized Hamilton matrix has (within the three-center approximation) the form

$$\begin{aligned} H_{11}^d &= E_0 + \Delta_{\text{Ni}}^V + 2\tilde{B}_1(\cos 2\xi + \cos 2\eta) - J_{ex}/2 \\ H_{22}^d &= E_0 + 2\tilde{B}_2 \cos 2\xi + 2\tilde{B}_3 \cos 2\eta - J'_{ex}/2 \\ H_{33}^d &= E_0 + 2\tilde{B}_3 \cos 2\xi + 2\tilde{B}_2 \cos 2\eta - J'_{ex}/2 \\ H_{44}^d &= E_0 + \Delta_{\text{Fe}}^V + 2\tilde{B}_4(\cos 2\xi + \cos 2\eta) - J'_{ex}/2 \\ H_{55}^d &= E_0 + \Delta_{\text{Ni}}^V + \Delta_{\text{Fe}}^V + 2\tilde{B}_5(\cos 2\xi + \cos 2\eta) - J_{ex}/2 \\ H_{45}^d &= H_{54}^d = H_{9,10}^d = H_{10,9}^d = 2\tilde{B}_6(\cos 2\xi - \cos 2\eta) \end{aligned} \quad (2)$$

and

$$\begin{aligned} H_{ii}^d &= H_{i-5,i-5}^d + J_{ex} \quad \text{for } i = 6, 10, \\ H_{ii}^d &= H_{i-5,i-5}^d + J'_{ex} \quad \text{for } i = 7, 8, 9. \end{aligned}$$

Here, $\xi = \frac{1}{2}k_x a$ and $\eta = \frac{1}{2}k_y a$ are the normalized components of the crystal momentum \mathbf{k} , a is the lattice constant of the simple quadratic monolayer. For qualitative results it is sufficient to use bulk values for the parameters of the paramagnetic bandstructure \tilde{B}_i , the crystal field parameter $\Delta_{\text{Fe/Ni}}^V$, and the spin splitting parameters J_{ex} and J'_{ex} . For Ni, the parameters are taken from Welling and Callaway^{26,27}, for Fe from Pustogowa *et al.*^{28,29}. The \tilde{B}_i and Δ^V are listed in the first column of table I. We have used $J_{ex} = 0.1$ eV and $J'_{ex} = 0.4$ eV for Ni and $J_{ex} = J'_{ex} = 1.78$ eV for Fe. Due to the higher symmetry in fcc or bcc bulk crystals, only one crystal field parameter Δ_{Fe}^V (Δ_{Ni}^V) appears in the corresponding Fe (Ni) bulk Hamiltonian. For the monolayer, one would have to consider three different Δ because of the reduced symmetry, but these parameters are not known. Hence, only $\Delta_{\text{Fe/Ni}}^V$ has been considered in Eq. (2). The influence of further crystal field effects on E_{anis} in the monolayer, which was stressed by Bruno¹⁰, is investigated in section III.C.

For a quantitative comparison with experiment, however, 4s-states have to be included (within the so-called “combined interpolation scheme”²¹) due to the strong overlap and hybridization between 3d- and 4s-bands in 3d transition metals. According to the pseudopotential

method by Harrison³⁰, the 4s-electrons are described by a set of plane waves

$$\psi_{\mathbf{K}_j\mathbf{k}}(\mathbf{r}) = \frac{1}{\sqrt{Nv}} e^{i(\mathbf{k}-\mathbf{K}_j)\cdot\mathbf{r}},$$

where the \mathbf{K}_j are a set of reciprocal lattice vectors. They have to be chosen such that at least the lowest eigenstates in the considered part of the two dimensional Brillouin zone (irreducible part, see below) are described. For simple quadratic monolayers, this yields $\mathbf{K}_1 = (0, 0)$, $\mathbf{K}_2 = \frac{2\pi}{a}(1, 0)$, $\mathbf{K}_3 = \frac{2\pi}{a}(0, 1)$, $\mathbf{K}_4 = \frac{2\pi}{a}(1, 1)$, $\mathbf{K}_5 = \frac{2\pi}{a}(-1, 0)$ and $\mathbf{K}_6 = \frac{2\pi}{a}(1, -1)$. To maintain the symmetry of the problem (and thus the correct occurrence of band degeneracies that turn out to be very important for E_{anis}), *symmetry factors* F_i ²¹ have to be introduced into the Hamilton matrix. This leads to

$$H_{ij}^s = \langle \psi_{\mathbf{K}_i\mathbf{k}} | H | \psi_{\mathbf{K}_j\mathbf{k}} \rangle = \begin{cases} V_{00} + \alpha(\mathbf{k} - \mathbf{K}_i)^2 & \text{for } i = j, \\ V_{\mathbf{K}_j - \mathbf{K}_i} F_i F_j & \text{else} \end{cases}$$

V_{00} , V_{10} , V_{11} , V_{12} and V_{02} are the Fourier components of the pseudopotential, α is the dispersion of the 4s-band. The symmetry factors are:

$$\begin{aligned} F_1 &= 1 \\ F_2 &= \sin 2\xi \\ F_3 &= \begin{cases} \sin 2\eta & \text{for } \eta \geq 0, \\ 0 & \text{else} \end{cases} \\ F_4 &= F_2 F_3 \\ F_5 &= \begin{cases} \sin 2\eta & \text{for } \eta \leq 0, \\ 0 & \text{else} \end{cases} \\ F_6 &= F_2 F_5 \end{aligned}$$

The *s-d* hybridization H^{sd} between states of parallel spins is calculated according to Hodges *et al.*²¹ with the parameters B_1 and B_2 . To obtain accurate parameters, we perform a fit to the full-potential linear muffin-tin orbitals (LMTO) calculation for a free-standing Fe monolayer by Pustogowa *et al.*³¹ and to the linear augmented plane wave (LAPW) calculation for a Ni monolayer by Jepsen *et al.*³². The resulting parameters are listed in table I. In order to reduce the number of free parameters in the fit, the *d*-band parameters \tilde{B}_i and Δ^V are still taken from the corresponding bulk crystals (see above). To obtain correct *d*-bandwidths, however, the \tilde{B}_i are scaled with the fitted parameters S^\uparrow and S^\downarrow for the spin-up and spin-down bands, respectively. Finally, the *s*- and *d*-bandwidths and *s-d*-hybridization parameters are scaled with t according to Harrison³³ to take into account the Cu surface lattice constant a :

$$\left(\frac{a}{a_0}\right)^q = \left(\frac{t}{t_0}\right) \quad (3)$$

with a_0 the surface lattice constant of Fe or Ni, t_0 the corresponding hopping parameters, and q being -5 for

the *dd* parameters, -2 for the *ss* parameters and -7/2 for the *sd* parameters. The in-plane lattice constant is taken to be that of the Cu-substrate for all considered systems ($a = 2.56$ rÅ). This is correct for Ni, which is known to have a large pseudomorphic growth range²². For Fe however, both an in-plane nearest-neighbor distance similar to that of Cu and a smaller one^{17,34} have been reported.

B. Spin-orbit coupling

Spin-orbit coupling (SOC) between the *d*-states, leading to magnetocrystalline anisotropy, is introduced in the usual form as $H_{so} = \lambda_{so} \mathbf{l} \cdot \mathbf{s}$. It can be expressed by the components of the orbital momentum operator \mathbf{l} in the rotated frame (x_M, y_M, z_M) ⁸. Here, z_M is the spin quantization axis, which is parallel to the direction of magnetization (θ, ϕ) ³⁵.

$$H_{so} =: \begin{pmatrix} H_{so}^{\uparrow\uparrow} & H_{so}^{\uparrow\downarrow} \\ H_{so}^{\downarrow\uparrow} & H_{so}^{\downarrow\downarrow} \end{pmatrix} = \frac{\lambda_{so}}{2} \begin{pmatrix} l_{z_M} & l_{x_M} - il_{y_M} \\ l_{x_M} + il_{y_M} & -l_{z_M} \end{pmatrix} \quad (4)$$

Expressed in the basis of Eq. (1), H_{so} is a matrix function of the magnetization direction (θ, ϕ) . The SOC constant λ_{so} is taken from the corresponding atom: $\lambda_{so} = 70$ meV for Ni and 50 meV for Fe³⁶.

Unlike in usual tight-binding calculations^{7,8,10,14}, SOC is included non-perturbatively³⁷ in our treatment. Thus, we obtain important new information on how E_{anis} scales with the SOC constant λ_{so} , which contributes to our analysis of the origin of E_{anis} in terms of bandstructure properties (see below).

C. Multilayers

We build up the Hamiltonian of a system of l layers by coupling l monolayer Hamiltonians $H_{mono}^{i=1\dots l}$ together. The coupling of the layers is described within the tight-binding nearest-neighbor formalism used for the monolayer. Because of the missing periodicity in *z*-direction, we obtain terms that depend only on ξ and η . For the sake of simplicity, we take only σ -bonds into account and obtain the following terms for the coupling of the orbital j of the monolayer i with the orbital k of the monolayer $i+1$, $H_{j,k}^{i,i+1}$:

$$\begin{aligned} H_{22}^{i,i+1} &= -2\tilde{B}_1 \cos 2\eta \\ H_{33}^{i,i+1} &= -2\tilde{B}_1 \cos 2\xi \end{aligned}$$

with $i=1\dots l$. The $(18l \times 18l)$ coupling matrix thus has only elements in the $(l-1)$ (18×18) -blocks just above and below the diagonal. The parameter \tilde{B}_1 is the same as used for the monolayers, but it yet has to be scaled to the interlayer distance of the tetragonally-distorted system, according to Eq. (3). We consider equidistant layers.

For Ni, we take into account the reported compression of 3.2% to scale the interlayer hoppings²². For Fe, we assume an expansion of about 5% as reported by Müller *et al.*¹⁸.

D. Anisotropy energy

The magnetic anisotropy energy per atom is defined as

$$E_{anis}(n) := E_{tot}(\theta = 0; n) - E_{tot}(\theta = \pi/2, \phi_0; n), \quad (5)$$

where $E_{tot}(\theta, \phi; n)$ is the ground-state energy per atom with a total of n $3d$ - and $4s$ -electrons per atom, and the magnetization direction is denoted by (θ, ϕ) ³⁵. The in-plane angle ϕ_0 is chosen such that the resulting $|E_{anis}|$ is the largest possible. At first, the anisotropic dipole-dipole interaction is neglected, since it does hardly depend on the electronic structure. Nevertheless, it may be of the same order of magnitude as the magnetocrystalline anisotropy resulting from SOC and will thus be included later to obtain quantitative results. The total energy per atom E_{tot} (with the \mathbf{k} -space resolved energy $E_{\mathbf{k}}$) is given by

$$\begin{aligned} E_{tot}(\theta, \phi; n) &= \frac{1}{N} \sum_{\mathbf{k}} E_{\mathbf{k}}(\theta, \phi; n) \\ &= \frac{1}{N} \sum_{m, \mathbf{k}} E_{m\mathbf{k}}(\theta, \phi) f_0(E_{m\mathbf{k}}(\theta, \phi) - E_F(\theta, \phi; n)). \end{aligned} \quad (6)$$

with N the number of atoms. $f_0(\Delta E)$ is the Fermi-function at zero temperature and $E_F(\theta, \phi; n)$ is the Fermi-energy which, for a given bandfilling n , is determined self-consistently by

$$n = \frac{1}{N} \sum_{m, \mathbf{k}} f_0(E_{m\mathbf{k}}(\theta, \phi) - E_F(\theta, \phi; n)).$$

$E_{m\mathbf{k}}(\theta, \phi)$ is the m -th eigenvalue with crystal momentum \mathbf{k} and magnetization along (θ, ϕ) of the Hamiltonian

$$H_{mono} = H^d + H_{so}$$

for the monolayer in the tight-binding scheme and

$$H_{mono} = H^s + H^d + H^{sd} + H_{so}$$

for the monolayer in the combined interpolation scheme. For multilayer systems, we have the following Hamiltonian:

$$H = H_{mono}^1 \oplus \dots \oplus H_{mono}^n + H_{coupling}$$

In Eq. (6), we use the so-called *force theorem*, the validity of which has been assumed in all calculations of the magnetocrystalline anisotropy so far.

The complete Brillouin zone (BZ) summation over \mathbf{k} is performed as a weighted summation over the irreducible

part of the BZ (for an arbitrary direction of magnetization). For the d -electrons with SOC, that means a summation over 1/4 of the BZ. About 2000 points of the 1/4 BZ are then sufficient to achieve convergence. Note that we do not have to exclude any parts of the BZ to obtain convergence, unlike Wang *et al.*¹². Adding s -electrons and s - d hybridization implies a coupling of non-SOC coupled states with the SOC-coupled d -states and results in a reduced symmetry. It is then necessary to perform the summation over 1/2 of the BZ. We then need 150 000 points to obtain the correct fourfold symmetry of the in-plane anisotropy energy as a function of the magnetization direction in the plane ($\cos 4\phi$). Fortunately, the out-of-plane anisotropy energy E_{anis} as defined by Eq.(5), which is larger by two orders of magnitude in our calculation ($E_{anis}^{in-plane} \simeq 1.2 \mu\text{eV}$ for Fe)³⁸ already converges for about 7000 points, so that calculations for systems of up to 14 layers are feasible.

III. RESULTS AND DISCUSSION

A. Monolayers within the tight-binding scheme

In Figs. 1 and 2, results for E_{anis} as a function of the $3d$ -bandfilling n_d are presented (solid lines) for the parameters of Fe and Ni monolayers, respectively. We use the lattice constant of 2.56 rÅ to simulate epitaxial growth on Cu(001). These figures demonstrate the correspondence between electronic structure and magnetic anisotropy and show that our method will yield convergent results for the whole transition metal series and for large (Fe) and small (Ni) exchange coupling. They will be analyzed in the following. Yet, the numerical value of E_{anis} for Fe and Ni monolayers cannot be extracted from these figures until the $4s$ -electrons are included (see III.C), since the exact $3d$ -bandfilling of the monolayers is not known.

Splitting the spin-orbit coupling matrix H_{so} into two parts, one of them (H_{so}^{par}) containing only coupling between states of parallel spin, the other one ($H_{so}^{antipar}$) between states of opposite spin, and recalculating E_{anis} as a function of n_d with either of the two matrices instead of H_{so} itself, we obtain the curves $E_{anis}^{par}(n_d)$ and $E_{anis}^{antipar}(n_d)$, respectively (Figs. 1 and 2, dashed and dotted lines respectively). Note that to a good approximation $E_{anis}^{par}(n_d) + E_{anis}^{antipar}(n_d) \approx E_{anis}(n_d)$ is valid. For Fe parameters, $E_{anis}^{antipar}(n_d)$ is very small due to the large exchange splitting J_{ex} that completely separates the spin subbands. Thus, $E_{anis}^{antipar}(n_d)$ is ineffective and may therefore be neglected for further analysis. The curve $E_{anis}^{par}(n_d) \approx E_{anis}(n_d)$ consists of two parts of equal shape, viz. for $n_d \in [0; 5]$ (spin-up band) and $n_d \in [5; 10]$ (spin-down band). In the case of Ni, $E_{anis}^{par}(n_d)$ and $E_{anis}^{antipar}(n_d)$ are of the same order of magnitude, since there is a considerable overlap between the spin-up and spin-down subbands.

The curves $E_{anis}(n_d)$ show a number of pronounced peaks (A, B, C, E, F in Figs. 1 and 2), the origin of which has to be clarified. Two possible contributions to E_{anis} are discussed in the literature^{11–13}: (i) The SOC-induced shifting of occupied, nondegenerate bands leads to contributions to E_{anis} in second-order perturbation theory with respect to the SOC constant λ_{so} : $E_{anis} \propto \lambda_{so}^2$. The first order vanishes due to time reversal symmetry¹⁰. (ii) The contribution of the lifting of degenerate bands, which are shifted linearly with λ_{so} , depends on the fraction of states in \mathbf{k} -space influenced by the degeneracy. Whether this fraction is of the order of λ_{so}^2 , which would yield¹² $E_{anis} \propto \lambda_{so}^3$, or this fraction is of lower order and thus would yield important contributions to E_{anis} ,^{11,13} has been a controversial question. Anyway, the scaling of E_{anis} with λ_{so} can present important information about the dominant contributions to E_{anis} . Thus, it is very useful not to restrict calculations to second order perturbation theory as has been frequently done^{10,14}. Remarkably, we find $E_{anis}(n_d) \propto \lambda_{so}^2$ for most of the n_d values in agreement with Wang *et al.*¹². Unlike stated by those authors, however, this does not rule out contributions to E_{anis} of the lifting of degeneracies (ii). In section III.B and Fig. 3, we show explicitly that such contributions play a very important role for E_{anis} in the monolayers considered. This is true as well for the multilayers (s. Figs. 13, 14, and 15 and the discussion in sections III.E and III.F).

The dependence of E_{anis} on scaling of all d -electron hopping parameters with a common parameter t was checked. We found that the overall shape of the curves $E_{anis}(n)$ will not change if t is varied. $|E_{anis}|$ increases for decreasing t (decreasing bandwidth). This leads to the general trend: $|E_{anis}|$ increases with increasing lattice constant a of the monolayer, since t is proportional to a^{-5} (see section III.C)³³.

B. The electronic origin of E_{anis}

In this chapter we discuss in detail how the magnetocrystalline anisotropy energy can be related to the electronic bandstructure. A $3d$ -band degeneracy can make large contributions to E_{anis} , if (i) it is lifted by SOC for one direction of magnetization (z_M^Ξ) and remains for another (z_M^X); (ii) it is located near the Fermi level E_F ; (iii) it runs along a line in \mathbf{k} -space and (iv) the degenerate bands have no or very little dispersion along this line. Before showing that such degeneracies indeed occur in the bandstructures, we estimate their contribution within a linearized 'bandstructure' (see Fig. 3). If E_F is situated below or above the two subbands, no contribution to E_{anis} results: $\Delta E_{anis} = 0$. The maximal contribution occurs when the degeneracy lies exactly at the Fermi level E_F and amounts to:

$$\Delta E_{anis} = \frac{\lambda_{so}}{2} F = \lambda_{so}^2 \left(\frac{\partial E}{\partial k_1} \frac{\pi}{a} \right)^{-1} \quad (7)$$

since the fraction F of involved states in the irreducible quarter of the BZ is $F = \frac{\Delta k_1}{\pi/a} \frac{\pi/a}{\pi/a} = 2\lambda_{so} \left(\frac{\partial E}{\partial k_1} \frac{\pi}{a} \right)^{-1}$. The preferred direction of magnetization is z_M^Ξ .

Thus, ΔE_{anis} is proportional to λ_{so}^2 for a degeneracy that occurs along a *line* with the involved bands being non-dispersive along that line. This agrees with the scaling of E_{anis} observed above. In their estimate of the contribution of degeneracies, Wang *et al.*¹² implicitly assume that the degenerate bands are dispersive in either dimension of \mathbf{k} -space. This would lead to $F \propto \lambda_{so}^2$ and $E_{anis} \propto \lambda_{so}^3$ and justify the exclusion of degeneracies from their calculation in order to improve convergence. In the light of our results, however, this assumption is incorrect and it neglects very important contributions to E_{anis} .

In Fig. 4, some degeneracies are shown in the bandstructure of the Fe monolayer. For example, the degeneracy A that occurs for $\mathbf{M} \parallel \hat{z}$ and is lifted for $\mathbf{M} \parallel \hat{x}$ is located at the Fermi level for $n_d = 7, 6$ (dotted lines in Fig. 4) and leads to the peak A in Fig. 1. It runs along a line in \mathbf{k} -space, which is shown Fig. 8. According to Eq. (7), with $\frac{\partial E}{\partial k_y} = 0.6 \text{ eV}/\frac{\pi}{a}$ (taken from the bandstructure), this contribution should be $\Delta E_{anis} \approx 4 \text{ meV}$, which agrees in the order of magnitude with the calculated value $E_{anis}(n_d = 7.6) = 6 \text{ eV}$.

Several tests have been made to support that hypothesis. Excluding the states influenced by the degeneracy A (4.3% of the total of $3d$ -states) from the calculation of E_{anis} , the height of peak A is reduced to 40%. The \mathbf{k} -space resolved analysis of $E_{anis}(n_d = 7.6)$ (Fig. 5) also shows clearly that E_{anis} results from the states near the degeneracy.

Analogous degeneracies are found in the Ni bandstructure contributing to the peaks E and F (Fig. 2). Note that the lifting of degeneracies can favor in-plane as well as perpendicular magnetization. This is in contradiction to the results of Daalderop *et al.* for a Co(111) monolayer¹³, who state that degeneracies should always favor perpendicular magnetization.

Since the $3d$ -band degeneracies are so important for E_{anis} , we analyze in the following the occurrence and lifting of degeneracies in the bandstructure. It can be shown that, in terms of the basis of Eq. (1), the Hamilton matrix H^d (Eq. (2)) has the simplest block diagonal form with only four off-diagonal elements (ODEs) $H_{45}^d = H_{54}^d$ and, equivalently, $H_{9,10}^d = H_{10,9}^d$. To find out which additional ODEs are introduced by SOC for a given direction of the magnetization \mathbf{M} , we analyze the form of H_{so} in Eq. (4). States with parallel spins are coupled if they contain equal orbital momenta with respect to the spin quantization axis z_M , whereas states with opposite spins must show a difference of one in the orbital momenta to yield nonvanishing ODEs. The real space components of the atomic states ϕ_i , $i = 1, \dots, 5$, are composed of eigenstates of l_z with the eigenvalues $(-2, 2)$,

$(-1,1)$, $(-1,1)$, $(-2,2)$ and 0, respectively. In terms of eigenstates of l_x one has the eigenvalues $(-1,1)$, $(-2,2)$, $(-1,1)$, $(-2,0,2)$ and $(-2,0,2)$, respectively. This yields a coupling for $\mathbf{M} \parallel \hat{z}$ within the groups of states ψ_i with $i = 1, 4, 5, 7, 8$ and with $i = 2, 3, 6, 9, 10$, and, in the case of $\mathbf{M} \parallel \hat{x}$, within the groups of states ψ_i with $i = 2, 4, 5, 6, 8$ and $i = 1, 3, 7, 9, 10$, respectively. In both cases, the Hamiltonian can be split into two 5×5 blocks, and subbands belonging to different blocks will intersect. Between states of the same block, the degeneracies will usually be removed. Especially the subbands ψ_1 and ψ_2 (and, correspondingly, ψ_6 and ψ_7) change their roles if the magnetization is changed from \hat{z} to \hat{x} and vice versa, because the orbitals xy and yz have different orbital momenta with respect to the x - and z -axes. These subbands will thus be involved in the lifting of degeneracies by altering magnetization and possibly, as shown above, yield important contributions to E_{anis} . In the case of Fe parameters, the situation is even simpler since coupling between states of opposite spin (ψ_i and ψ_j with $i \leq 5 < j$) can be neglected.

As an example, peak *A* in the curve $E_{anis}(n)$ of Fe at $n = 7.6$ (Fig. 1) results from the degeneracy *A* (Fig. 4) of the subbands corresponding to the states ψ_7 and (ψ_9, ψ_{10}) . Thus, it occurs for $\mathbf{M} \parallel \hat{z}$, and is lifted for $\mathbf{M} \parallel \hat{x}$, since in the second case the subbands belong to the same block of the Hamiltonian, whereas in the first they do not.

As a conclusion, it has been shown that $3d$ -band degeneracies along lines of constant energy result in important contributions to E_{anis} if they occur near the Fermi level. They can favor in-plane and perpendicular magnetization and need not occur near high symmetry points of the BZ. Thus, for (001) layers, it is not sufficient to consider only bands at high symmetry points as was done by Daalderop *et al.*¹³ for a Co(111) monolayer. Furthermore, for such contributions from degeneracies, $E_{anis} \propto \lambda_{so}^2$ and, approximately, $E_{anis} \propto 1/\frac{\partial E}{\partial k_1}$ is valid (the band dispersion $\frac{\partial E}{\partial k_1}$ is approximately proportional to the scaling t of the hopping parameters) which agrees with the observations reported above. Note that the analysis is very simple due to the analytic form and low dimension of the $3d$ tight-binding matrix, which is an advantage of the semiempirical scheme. It remains valid if the extension to s -states is performed (see below).

C. The results of the combined interpolation scheme

Results for $E_{anis}(n)$ obtained from the combined interpolation scheme (including s - and d -bands as well as s - d hybridization) for the monolayer are presented in Fig. 6 for Fe parameters and Fig. 7 for Ni parameters with the lattice constant of the Cu(001) surface in both cases (solid curves; the discussion of the curves for two and three layers is postponed to section III.E and III.F). These results for the monolayer are similar to the curves

for d -bands only (Figs 1 and 2). n is the total filling of the s - and d -band ($n = 8$ for Fe and $n = 10$ for Ni). We find for a Fe monolayer $E_{anis}(\text{Fe/Cu}) = -0.41$ meV per atom, for Ni $E_{anis}(\text{Ni/Cu}) = 0.10$ meV per atom. The dipole-dipole interaction is included under the assumption of a point dipole located at each site, carrying the magnetic moment of the unit cell. The (spin) magnetic moment per atom is calculated from the bandstructure ($m(\text{Fe/Cu}) = 3.3\mu_B$ and $m(\text{Ni/Cu}) = 0.91\mu_B$). The dipole anisotropy (equivalent to the shape anisotropy in the monolayer) always prefers in-plane magnetization. Altogether, we obtain for the total magnetic anisotropy energy per atom of a Fe and Ni monolayer with the lattice constant of Cu(001)

$$E_{anis}^{tot}(\text{Fe/Cu}) = -0.17 \text{ meV} \quad \text{and} \\ E_{anis}^{tot}(\text{Ni/Cu}) = 0.12 \text{ meV}$$

with the easy axis perpendicular to the monolayer for Fe and in-plane for Ni. Note that corresponding *ab-initio* results for a free-standing Fe-monolayer yielded -0.42 meV^{9,12}, but previous tight-binding calculations gave the too large value of -5.5 meV¹⁴.

In the case of Fe, the perpendicular easy axis of ultra-thin Fe films on Cu(001) is reproduced correctly. Direct comparison with a Fe monolayer on Cu(001) is difficult due to film growth problems⁴. It is common use to separate the anisotropy energy of thin films in a volume and a surface term^{5,22}:

$$E_{anis}(d) = \mathbf{K}_v + \frac{2\mathbf{K}_s}{d}, \quad (8)$$

The first term, \mathbf{K}_v , describes the thickness independent contributions to the anisotropy energy, and the second, \mathbf{K}_s , the thickness dependent contributions and the surface effects. Fowler and Barth measure the following anisotropy constants⁵: $\mathbf{K}_v = 0.132$ meV/atom and $\mathbf{K}_s = 0.11$ meV/atom for the distorted fcc-films at 100 K. The value $\mathbf{K}_v + 2\mathbf{K}_s = 0.352$ meV/atom is comparable to our result. This result has been calculated with the measured anisotropy field using the bulk saturation magnetization of bcc-Fe. For Ni, our result also agrees very well with experiments²² which yields $E_{anis}(\text{Ni/Cu}) = 0.125$ meV at 300 K. The anisotropy constants \mathbf{K}_s and \mathbf{K}_v are temperature dependent. Measurements of the anisotropy constants as a function of the reduced temperature have been made³⁹, but the correct extrapolation to $T=0$ K is not known yet. While in experiment, the values of K_v and K_s have to be compared at the same reduced temperature because of the thickness dependence of T_c , the theoretical values are for 0 K and thus independent of the difference of absolute and reduced temperature.

Note that in Fig. 7, the curve $E_{anis}(n)$ for the Ni monolayer (solid curve) has zeros near $n = 10$. Hence, the numerical result for Ni is not very stable and the excellent agreement with experiment should not be overemphasized. Nevertheless, for Fe and Ni, the sign and the order

of magnitude of E_{anis} turn out to be remarkably stable upon parameter variations: Sign changes do not occur upon variation of the pseudopotential and s - d hybridization parameters by as much as 40%. Moreover, we find in agreement with Wang *et al.*¹² a perpendicular easy axis also for Fe monolayers taking (001) surface lattice constants imposed by substrates such as Pd, Ag, and V (2.77 rA, 2.89 rA, and 3.03 rA), respectively. This stability again demonstrates the validity of our results for E_{anis} . The good agreement of the results both with *ab-initio* theories and experiments is due to the fact that the parameters were obtained by a fit to *ab-initio* calculations for Fe and Ni *monolayers* rather than taking *bulk* parameters.

To investigate crystal field effects, an additional parameter Δ is introduced¹⁰ to take into account the different effect of the monolayer geometry on orbitals that lie in the plane of the monolayer (xy and $x^2 - y^2$) and out-of-plane orbitals (yz , zx and $3z^2 - r^2$). Additional to Eq. (2), the on-site energies of the latter are lowered by Δ with respect to the first. The dependence of E_{anis} on Δ is shown in Fig. 9 for Fe and Ni parameters (solid and dashed curve, respectively). Remarkably, $\Delta = 0.2$ eV changes the sign of E_{anis} for both systems considered. Thus, it is important to determine Δ from the *ab-initio* bandstructures. In the case of Fe, the fit of the $3d$ -bands near the $\bar{\Gamma}$ -point of the BZ can be significantly improved by choosing $\Delta = 0.08$ eV. The resulting $E_{anis}(\text{Fe/Cu})$ amounts to -0.30 meV, still with perpendicular easy axis even if the dipole-dipole interaction is added. For Ni, the introduction of Δ does *not* improve the fit. Those results for Δ differ substantially from $\Delta = -0.5$ eV given by Bruno¹⁰ which has been determined by a fit to the Ni(111) monolayer but employed for both Fe and Ni(001) monolayers also. Pick and Dreyss¹¹ state that for (001)-monolayers a crystal field parameter is not necessary. For Ni, this is supported by our result; even in Fe, our value of Δ is small compared to other bandstructure parameters. Cinal *et al.*¹⁴ report $\Delta = -0.14$ eV for the Ni(001) monolayer.

Finally, a detailed investigation of the bandstructures²⁵ shows that the analysis given in section III.B for $3d$ -bands only is still valid for the combined interpolation scheme. As an evidence, consider Figs 1 and 6 (solid curves): There is a one-to-one correspondence between the peaks in E_{anis} in both curves. This correspondence can be shown to result from similar bandstructure details. In particular, the role of $3d$ -band degeneracies stressed in section III.B remains the same in the complete scheme.

D. Temperature dependence

One of the greatest challenges in the investigation of magnetic anisotropy is the calculation of reorientation transitions with temperature. Up to now, a complete electronic and thermodynamic theory is lacking. Here,

one-particle effects of temperature are investigated. It turns out that they again support the role of degeneracies for magnetic anisotropy and, moreover, are comparable in order of magnitude with the many-particle aspects usually considered⁴⁰.

The free magnetic anisotropy energy F_{anis} depends on temperature T due to (i) the Fermi distribution of electronic states $f_T(\Delta E)$, (ii) the hopping integrals, which depend on T because of the lattice expansion of the substrate, (iii) the entropy $S(T)$ and (iv) the effects of spin-waves, resulting in a temperature dependence of the magnetization $\mathbf{M}(T)$. In this work, the first three effects are analyzed. More precisely, the thermal expansion (ii) of the lattice constant $a(T)$ is included by means of the empirical law $a(T) = a(T=0)(\alpha T + 1)$. $\alpha = 2 \cdot 10^{-5}/\text{K}$ is the expansion coefficient for the Cu substrate⁴¹. The expression for the entropy (iii) of non-interacting particles is:

$$S = -k_B \sum_{m,\mathbf{k}} \langle n_{m\mathbf{k}} \rangle \ln \langle n_{m\mathbf{k}} \rangle + (1 - \langle n_{m\mathbf{k}} \rangle) \ln(1 - \langle n_{m\mathbf{k}} \rangle)$$

with $\langle n_{m\mathbf{k}} \rangle = f_T(E_{m\mathbf{k}}(\theta, \phi) - \mu(\theta, \phi; n))$. In analogy to Eq. (5), the free magnetocrystalline anisotropy energy F_{anis} is defined as the difference in the free energy $F = E - TS$ for two different directions of magnetization.

Fig. 10 shows $F_{anis}(T)$ (d -band calculation for the monolayer, Fe parameters, $n_d = 6$). Including only Fermi statistics (i; dashed curve), the characteristic energy scale for the decrease of $|F_{anis}|$ with T is about 1000 K (100 meV), which corresponds to the energy $2\lambda_{so}$, but not to the $3d$ -bandwidth of approximately 3 eV. This becomes immediately plausible if one notices that the SOC-induced lifting of degeneracies occurs near the Fermi level. Thus, one expects a measurable effect on F_{anis} due to Fermi statistics as soon as $k_B T$ becomes larger than or comparable to $2\lambda_{so}$. In addition, we must conclude from our results that shifting of subbands far below the Fermi-level is not so important, since then F_{anis} could not be essentially lowered on such a small temperature scale.

The characteristic increase of $|F_{anis}|$ with increasing temperature for $T < 500$ K is a direct result of the lifting of degeneracies. Consider again Fig. 3: for $\mathbf{M} \parallel z_M^{\bar{\bar{z}}}$ (lifted degeneracy), which is the energetically favored case, Fermi statistics induces only little changes in the occupation of the electronic states, if $k_B T < \lambda_{so}$; for the degenerate bands ($\mathbf{M} \parallel z_M^X$), however, states in the upper band are significantly occupied even for $k_B T < \lambda_{so}$. Thus, the total energy for $\mathbf{M} \parallel z_M^X$ rises with respect to $T = 0$ in this temperature range. This leads to an increase of $|F_{anis}|$ with increasing T , if $k_B T < \lambda_{so} = 50$ meV ($T < 500$ K).

The inclusion of lattice expansion (ii; solid curve in Fig. 10) has only a small effect on F_{anis} . The narrowing of bands with increasing temperature due to the scaling of the hoppings leads to an increase in $|F_{anis}|$ for *small* T , which was already discussed for $T = 0$. For *larger*

T , the influence of Fermi statistics on narrowed bands is larger, leading to a stronger decrease of $|F_{anis}|$.

The entropy (iii; dotted curve) has a damping effect on the curve $F_{anis}(T)$, but maintains the features discussed above. This results from the fact that, in the case of degenerate bands, the entropy is larger than for nondegenerate bands, since states located nearer to the Fermi level have larger entropy.

$F_{anis}(T)$ was also calculated for bilayers (Fig. 11), taking into account all three mentioned effects and shows a decrease with increasing temperature on the same scale as for the monolayer. Hence, this analysis of $F_{anis}(T)$ shows the significant contribution of temperature-induced changes of the degeneracies to the anisotropy energy. It is remarkable that the three temperature effects mentioned above, and particularly the electron temperature dependence of the Fermi-function, are of equal magnitude as the temperature effects of spin-waves on $\mathbf{M}(T)$.

E. Fe Multilayers

Fig. 12 shows the calculated magnetic anisotropy energy for Fe films of 1 to 14 layers. Calculations for both $1/4$ BZ and $1/2$ BZ are included. The values obtained when the summation over \mathbf{k} is performed over $1/4$ BZ lead to periodically recurring positive values of E_{anis} (for films of 2, 6, 9 and 12 layers). The positive value for film of 2 layers can be traced back to the occurrence of degeneracy A at the Fermi-level. For the other positive values, easy and hard axis are found to be in-plane, an effect of the wrong symmetry resulting from the summation over $1/4$ BZ, and the following overestimation of the *in-plane* anisotropy $\mathbf{E}_{anis}^{in-plane}$. A new degeneracy D is found to be responsible for the negative values. In Fig. 13, we show the band structure of the Fe monolayer calculated within the combined interpolation scheme. The degeneracy A observed for the monolayer in the tight-binding scheme is easy to recognize, and a new degeneracy D is found near the M-point for $\mathbf{M} \parallel \hat{x}$. Degeneracy D is lifted for $\mathbf{M} \parallel \hat{z}$, thus leading to a negative anisotropy energy. The \mathbf{k} -space resolved anisotropy energy shown in Fig. 14 confirms the importance of degeneracy D, which causes the ring-shaped dip around M. The structure seen along the line LL' (s. Fig. 8) is the onset of the positive peak in the anisotropy energy caused by degeneracy A (s. Fig. 6). Summation of the contributions of the \mathbf{k} -points in the tenth of the BZ near M already gives half of the total anisotropy energy. Multilayer systems show per se more degeneracies than monolayers, and the contribution of these to the total anisotropy energy is not as clear as for the monolayer. Still, for a three layer system, we find again degeneracy D at the Fermi level, and recognize in the \mathbf{k} -space resolved anisotropy energy (Fig. 15) the characteristic structure it causes around M. We perform the \mathbf{k} -space summation again, this time

over $1/2$ BZ, thus respecting the symmetry of the s-d hybridized system. This reduces the importance of degeneracy A and we find positive values only at 2 and 6 ML. Taking Fig. 12 again and excluding the points of wrong symmetry (easy and hard axis in-plane) and the points where we find degeneracy A at the Fermi-level, we obtain the curve shown in Fig. 16. \mathbf{E}_{anis} is plotted as a function of $1/l$. We expected a linear behavior (s. Eq. (8)) and thus performed a linear least-square fit to the data. We then obtain $\mathbf{K}_v = -0.17$ meV per atom and $\mathbf{K}_s = -0.28$ meV per atom, which is in very good agreement with Fowler und Barth⁵.

Including the dipole-dipole anisotropy energy as calculated by L. Szunyogh *et al.*¹⁵, we would expect for Fe a change of the easy-axis from perpendicular to in-plane at 4 ML ($E_{anis}^{dip}(4 \text{ layers}) = 0.59 \text{ meV}$). Our result indicates that the experimentally observed transition at 5 ML might be an intrinsic quality of fct-films grown at low temperature. L. Szunyogh *et al.* calculated the anisotropy energy of thin fcc-Fe films on Au (001) and also observed oscillations. They obtained a reorientation transition from perpendicular to in-plane magnetization at 4 ML.

The dependence of E_{anis} of Fe on the $3d$ - and $4s$ -bandfilling n is shown in Fig. 6. For the monolayer at a s - and d -bandfilling $n=8$, we are near a zero of the curve, and at $n=8.2$ we already have a positive value of E_{anis} caused by the growing influence of degeneracy A. We would thus expect a monolayer of a Fe_xCo_{1-x} alloy to have an in-plane magnetization already at small Co concentrations. This was in fact measured by Dittschar *et al.*⁴² for $x=0.95$. We would predict an increase of the anisotropy energy with increasing Co concentration. For 3 layers, we would expect the same behavior, the structure of the curve $\mathbf{E}_{anis}(n)$ near $n=8$ being similar to that of the monolayer. This alloying behavior found both theoretically and experimentally supports the relevance of degeneracies for the anisotropy energy, as claimed by Daalderop *et al.* and disputed by Wang, Wu and Freeman. In this case, there is no doubt that the magnetic moment persists.

F. Ni Multilayers

The magnetic anisotropy of Ni calculated for systems of 1 to 14 ML is shown in Fig. 7. We include again calculations using $1/4$ of the BZ and $1/2$ BZ, but this time no point has to be excluded. \mathbf{E}_{anis} of the second layer is much bigger than that of the monolayer, a fact which indicates that the influence of the substrate maybe cannot be neglected. The anisotropy then sinks again and remains approximately constant at a value of about 0.14 meV (which is still bigger as the value obtained for the monolayer). Schulz and Baberschke²² report for Ni a transition from in-plane to perpendicular magnetization at 7 ML, due to a large \mathbf{K}_v which favors perpendicular

orientation of the magnetization. Our theory does not reproduce this reorientation.

For Fe, the behavior of the films as a function of thickness could be related to the degeneracies occurring at the Fermi-level. The contribution of these degeneracies to the total anisotropy of the film would be expected to decrease with increasing number of layers, as their weight in the summation over all atoms (number of points in the BZ \times number of layers) decreases: that is in fact what we find for Fe. For Ni, the contribution of the degeneracies to the anisotropy energy is not so evident, the minority and majority spin bands mix much more than in the case of Fe because of the small exchange coupling. This is a possible reason for the nearly constant anisotropy energy we obtain. The occurrence of a degeneracy of a l -times degenerated band would also probably lead to a thickness independent contribution to \mathbf{E}_{anis} .

So far, no other monolayer calculation lead to the correct in-plane anisotropy for the Ni-monolayer. In a calculation for the fct-bulk, Eriksson⁴³ finds a perpendicular easy-axis, which is correct for fct-Ni, but wrong for fcc-Ni. We obtain the correct in-plane anisotropy for the monolayer, but the wrong \mathbf{K}_v . So, a 3D calculation for fct-Ni does not really tackle the problem and explain the behavior of the magnetization.

Ni is a delicate system. Maybe many-body effects cannot be neglected (i.e. the *force theorem* does not work well). However, a total-energy calculation made by Eriksson⁴⁴ still yields the wrong sign for \mathbf{E}_{anis} for fcc-Ni bulk. The dependence between the anisotropy energy and the bandstructure seem to be very subtle and the smallest details can influence the results.

IV. CONCLUSIONS

A calculation of the magnetocrystalline anisotropy energy E_{anis} of Fe and Ni monolayers on Cu(001) is performed. In agreement with experiments, we find a perpendicular easy axis for Fe and an in-plane easy axis for Ni. The results are fully converged without any additional assumption to improve convergence. SOC is included non-perturbatively. It is an important result that large contributions to E_{anis} can result from the SOC-induced lifting of degeneracies occurring along *lines* in \mathbf{k} -space at the Fermi-level. The contributions of those degeneracies scale with the square of the SOC constant λ_{so} , as contributions from nondegenerate bands do. The occurrence and lifting of degeneracies in the $3d$ -band has been discussed in general. Evidence for the important contribution to \mathbf{E}_{anis} of the degeneracies at the Fermi-level are (i) the groove and the ring-shaped dip in the \mathbf{k} -space resolved anisotropy for the monolayer in the tight-binding scheme and in the combined interpolation scheme respectively, (ii) the temperature dependence (the characteristic energy scale for the decrease of the free magnetocrystalline anisotropy energy $|F_{anis}|$ as a function of

the temperature is determined by λ_{so}), (iii) the finite anisotropy energy at \mathbf{T}_c and (iv) the alloying behavior of Fe_xCo_{1-x} . We obtain for Fe a reorientation transition from perpendicular to in-plane magnetization at 4 ML, reorientation which is independent of any restructuring of the fct-film. Since it can be seen from Fig. 6 and Fig. 7 that both Fe and Ni do not exhaust the maximal anisotropy possible, our calculation of E_{anis} should also be important for the technologically relevant maximization of magnetic anisotropy by appropriate surface-alloy formation.

-
- ¹ J. H. Van Vleck, Phys. Rev. **52**, 1178 (1937).
 - ² M. L. Néel, J. Phys. Radium **15**, 225 (1954).
 - ³ R. Druzinic and W. Hübner, submitted for publication, 1996.
 - ⁴ D. P. Pappas, K.-P. Kämper, and H. Hopster, Phys. Rev. Lett. **64**, 3179 (1990); J. Thomassen *et al.*, Phys. Rev. Lett. **69**, 3831.
 - ⁵ D.E. Fowler and J.V. Barth, Phys. Rev. B **53**, 5563 (1996).
 - ⁶ Li *et al.*, Phys. Rev. Lett. **72**, 3112 (1994).
 - ⁷ A. J. Bennett und B. R. Cooper, Phys. Rev. B **3**, 1642 (1971).
 - ⁸ H. Takayama, K.-P. Bohnen und P. Fulde, Phys. Rev. B **14**, 2287 (1976).
 - ⁹ J. G. Gay and R. Richter, Phys. Rev. Lett. **56**, 2782 (1986).
 - ¹⁰ P. Bruno, Phys. Rev. B **39**, 865 (1989).
 - ¹¹ Š. Pick und H. Dreyssé, Phys. Rev. B **46**, 5802 (1992); Phys. Rev. B **48**, 13588 (1993); Š. Pick *et al.*, Phys. Rev. B **50**, 993 (1994).
 - ¹² Ding-sheng Wang, Ruqian Wu, and A. J. Freeman, Phys. Rev. Lett. **70**, 869 (1993); Phys. Rev. B **47**, 14932 (1993); Phys. Rev. Lett. **71**, 2166 (1993).
 - ¹³ G. H. O. Daalderop, P. J. Kelly and M. F. H. Schuurmans, Phys. Rev. Lett. **71**, 2165 (1993); Phys. Rev. B **41**, 11319 (1990); Phys. Rev. B **42**, 7270 (1990); Phys. Rev. B **50**, 9989 (1994).
 - ¹⁴ M. Cinal, D. M. Edwards, and J. Mathon, Phys. Rev. B **50**, 3754 (1994).
 - ¹⁵ L.Szunyogh, B. Újfalussy and P. Weinberger, Phys. Rev. B **51**, 9552 (1995).
 - ¹⁶ D.M. Bylander, Leonard Kleinman, Phys. Rev. B **52**, 1437 (1995); M. Weinert, R. E. Watson, J. W. Davenport, Phys. Rev. B **32**, 2115 (1985).
 - ¹⁷ J.V. Barth and D.E. Fowler, Phys. Rev. B **52**, 11432 (1995).
 - ¹⁸ S. Müller *et al.*, Phys. Rev. Lett. **74**, 765 (1995).
 - ¹⁹ M. Zharnikov *et al.*, Phys. Rev. Lett. **76**, 4620 (1996).
 - ²⁰ J. Hunter Dunn, D. Arvanitis, N. Martensson, preprint.
 - ²¹ L. Hodges, H. Ehrenreich, and N. D. Lang, Phys. Rev. **152**, 505 (1966).
 - ²² B. Schulz und K. Baberschke, Phys. Rev. B **50**, 13467 (1994).
 - ²³ G. C. Fletcher, Proc. Phys. Soc. **65**, 192 (1952).
 - ²⁴ J. C. Slater and G. F. Koster, Phys. Rev. **94**, 1498 (1954).

- ²⁵ T. H. Moos, Diploma thesis, Freie Universität Berlin (1995).
- ²⁶ F. Weling und J. Callaway, Phys. Rev. B **26**, 710 (1982).
- ²⁷ The parameters A_i used by Weling and Callaway have to be transformed into the coordinate system used here by
- $$\begin{aligned}\tilde{B}_1 &= A_4, & \tilde{B}_4 &= -A_1, \\ \tilde{B}_2 &= A_2 - A_3, & \tilde{B}_5 &= -\frac{1}{3}(A_4 + 4A_5), \\ \tilde{B}_3 &= A_2 + A_3, & \tilde{B}_6 &= \frac{2}{\sqrt{3}}A_6\end{aligned}$$
- and $J_{ex} = J_{ex}(e_g)$, $J'_{ex} = J_{ex}(t_{2g})$.
- ²⁸ U. Pustogowa, W. Hübner und K. H. Bennemann, Phys. Rev. B **48**, 8607 (1993).
- ²⁹ The corresponding transformation formulas are
- $$\begin{aligned}\tilde{B}_1 &= A_1, & \tilde{B}_4 &= \left(\frac{3}{4}A_4 + \frac{1}{4}A_2\right), \\ \tilde{B}_2 &= A_2, & \tilde{B}_5 &= \left(\frac{1}{4}A_4 + \frac{3}{4}A_2\right), \\ \tilde{B}_3 &= A_1, & \tilde{B}_6 &= \frac{\sqrt{3}}{4}(A_2 - A_4)\end{aligned}$$
- and $J'_{ex} = J_{ex}$.
- ³⁰ W. A. Harrison, *Pseudopotentials in the Theory of Metals* (Benjamin, Reading/Massachusetts, 1966).
- ³¹ U. Pustogowa, W. Hübner, K. H. Bennemann, and T. Kraft (unpublished).
- ³² O. Jepsen, J. Madsen und O. K. Andersen, Phys. Rev. B **26**, 2790 (1982).
- ³³ W. A. Harrison, *Electronic Structure and the Properties of Solids* (Freeman, San Francisco, 1980).
- ³⁴ S. Müller *et al.*, Phys. Rev. Lett. **75**, 2859, 1995; A.P. Bad-dorf, A.K. Swan, and J.F. Wendelken, Phys. Rev. Lett. **76**, 3658, 1996; K. Robinson *et al.*, Phys. Rev. Lett. **76**, 3659, 1996; S. Müller *et al.*, Phys. Rev. Lett. **76**, 3660, 1996.
- ³⁵ θ denotes the angle between the magnetization direction z_M and the surface normal \hat{z} . ϕ is the angle between the x -axis and the projection of z_M in the plane of the mono-layer.
- ³⁶ P. N. Argyres, Phys. Rev. **97**, 334 (1955).
- ³⁷ Of course, SOC *itself* is part of a perturbation expansion, leading from the Dirac equation to the Pauli equation.
- ³⁸ A. Lessard, diploma thesis, 1996.
- ³⁹ M. Farle *et al.*, Proceedings of E-MRS 1996, J. Magn. Magn. Mat. 1996.
- ⁴⁰ P. J. Jensen und K. H. Bennemann, Phys. Rev. B **42**, 849 (1990).
- ⁴¹ A. McB. Colliou und D. J. Powney, *The Mechanical and Thermal Properties of Solids* (Edward Arnold, London, 1973).
- ⁴² A. Dittschar *et al.*, J. Applied Phys. **79**, 5618, 1996.
- ⁴³ Eriksson, unpublished.
- ⁴⁴ J. Trygg, B. Johansson, O. Eriksson, and J.M. Wills, Phys. Rev. Lett. **75**, 2871, 1995.

TABLE I. Bandstructure parameters within the combined interpolation scheme for Fe and Ni (001)-monolayers with lattice constant a . The parameters \tilde{B}_i and Δ^V are taken from Pustogowa *et al.*^{28,29} for Fe and from Weling and Callaway^{26,27} for Ni (bulk parameters). The other parameters are obtained from a fit to *ab-initio* calculations for freestanding (001)-monolayers by Pustogowa *et al.*³¹ for Fe and Jepsen *et al.*³² for Ni.

	Fe	Ni
\tilde{B}_1 (eV)	0.0774	0.152923
\tilde{B}_2 (eV)	-0.00816	-0.015135
\tilde{B}_3 (eV)	0.0774	0.227635
\tilde{B}_4 (eV)	-0.15324	-0.25
\tilde{B}_5 (eV)	-0.05652	-0.071149
\tilde{B}_6 (eV)	0.08376	0.119380
Δ^V (eV)	0.068	0.059360
S^\uparrow	2.06	1.33
S^\downarrow	2.63	1.52
J_{ex} (eV)	2.18	0.87
J'_{ex} (eV)	2.18	1.17
E_0 (eV)	-0.54	-0.935
α (eV)	20.0	25.2
V_{00} (eV)	-4.20	-4.60
V_{10} (eV)	1.2	0.4
V_{11} (eV)	1.0	2.0
B_1 (eV)	7.5	5.0
B_2 (eV)	5.1	12.8
a (rÅ)	2.76	2.49

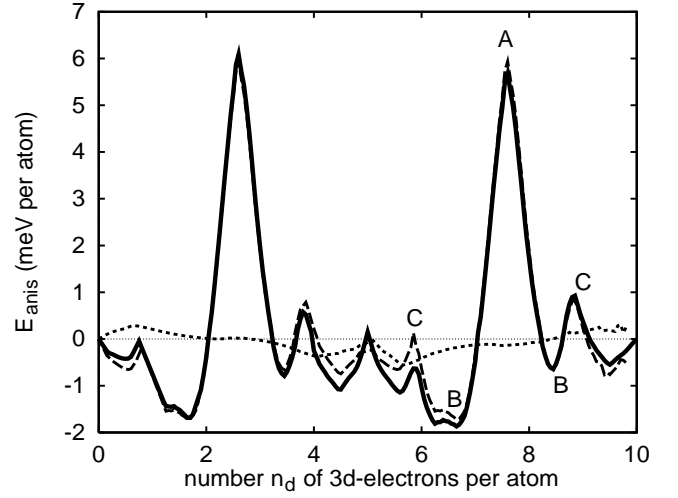


FIG. 1. Dependence of the magnetocrystalline anisotropy energy E_{anis} on the 3d-bandfilling n_d for a monolayer with parameters referring to Fe, calculated within the tight-binding scheme (solid curve). Negative values of E_{anis} yield perpendicular anisotropy. The origin of the peaks denoted by A, B and C can be traced back to degeneracies in the bandstructure (see text and Fig. 4). The dashed and dotted curves show the contributions E_{anis}^{par} and $E_{anis}^{antipar}$ to E_{anis} from the spin-orbit coupling between parallel spins and antiparallel spins, respectively.

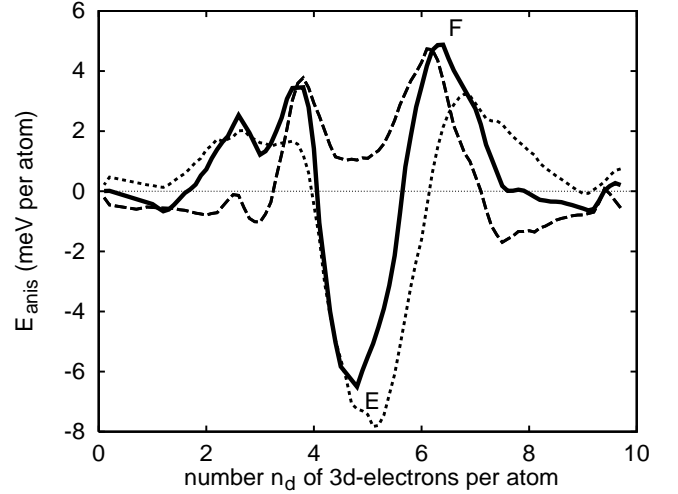


FIG. 2. Dependence of the magnetocrystalline anisotropy energy E_{anis} on the 3d-bandfilling n_d for a monolayer with parameters referring to Ni, calculated within the tight-binding scheme (solid curve). Negative values of E_{anis} yield perpendicular anisotropy. The origin of the peaks denoted by E and F can be traced back to degeneracies in the bandstructure (see text). The dashed and dotted curves show the contributions E_{anis}^{par} and $E_{anis}^{antipar}$ to E_{anis} from the spin-orbit coupling between parallel spins and antiparallel spins, respectively.

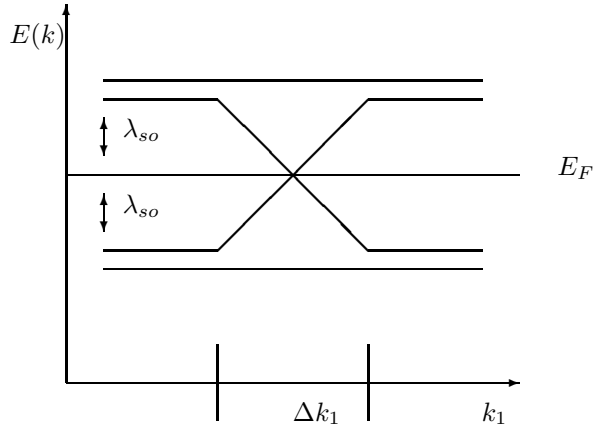


FIG. 3. Occurrence (full lines) and lifting (dashed lines) of a “line” degeneracy for two different directions of magnetization z_M^X and z_M^E , respectively. k_1 corresponds to one particular direction in k -space. Perpendicular to k_1 the intersecting bands are non-dispersive throughout the BZ. Note, the energy gained by the lifting of this degeneracy is given by $\Delta E_{anis} = \frac{1}{2} \lambda_{so} \cdot F$, if E_F falls in between the two subbands (dotted line). Here, F is the fraction of the involved states in k -space. Apparently, if E_F lies below or above the two subbands, ΔE_{anis} is zero.

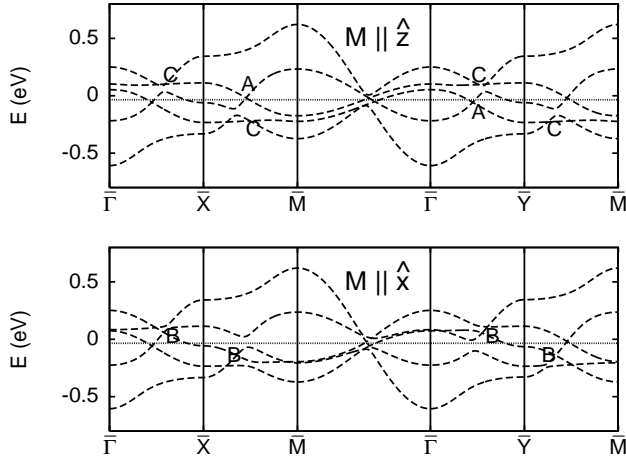


FIG. 4. Bandstructure of the 3d minority spin band of the Fe monolayer, calculated within the tight-binding scheme. The magnetization \mathbf{M} is directed along the layer normal \hat{z} (upper part) and in-plane along \hat{x} (lower part). The degeneracies denoted by A, B and C contribute to the peaks A, B and C in Fig. 1. The dotted lines denote the Fermi level for $n_d = 7, 6$, respectively. $\bar{\Gamma} = (0, 0)$, $\bar{X} = (\pi/a, 0)$, $\bar{Y} = (0, \pi/a)$ and $\bar{M} = (\pi/a, \pi/a)$ are the high symmetry points of the irreducible part ($0 \leq k_x, k_y \leq \pi/a$) of the Brillouin zone. a is the lattice constant of the monolayer.

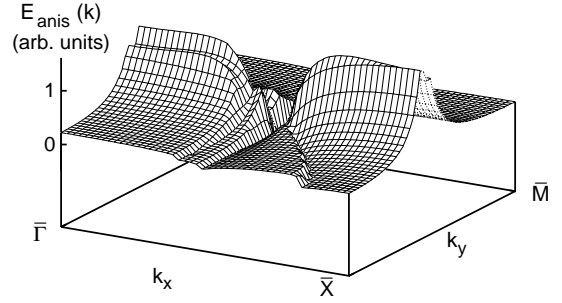


FIG. 5. k -space resolved magnetocrystalline anisotropy energy $E_{anis}(\mathbf{k}, n_d) = E_{\mathbf{k}}(\theta = 0; n_d) - E_{\mathbf{k}}(\theta = \pi/2, \phi = 0; n_d)$ in the irreducible part of the Brillouin zone ($0 \leq k_x, k_y \leq \pi/a$; a is the lattice constant of the monolayer) for the bandstructure of the Fe monolayer, $n_d = 7.6$ electrons per atom in the d -band, calculated within the tight-binding scheme. Positive values of $E_{anis}(\mathbf{k}, n_d)$ favor in-plane magnetization.

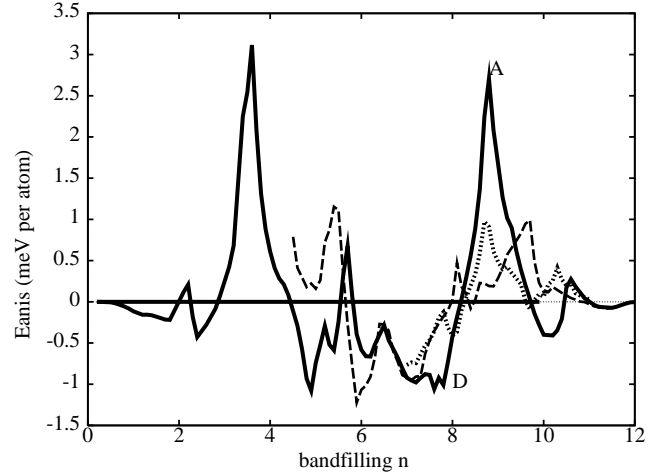


FIG. 6. Magnetic anisotropy energy of Fe as a function the s - and d -bandfilling for 1 layer (solid curve), 2 layers (dashed) and 3 layers (dotted). Peaks A and D are caused by the respective degeneracies in the bandstructure shown in Fig. 13.

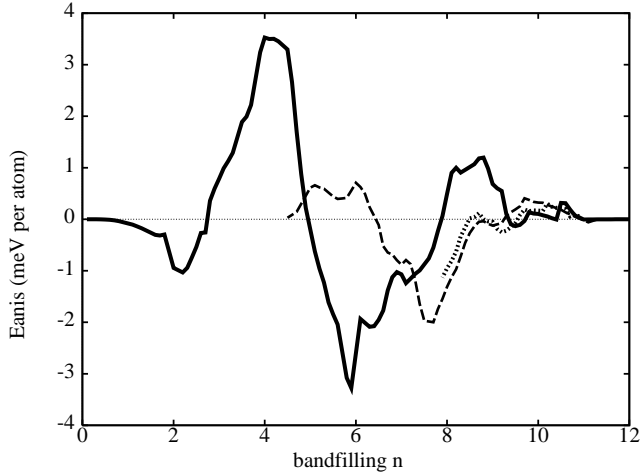


FIG. 7. Magnetic anisotropy energy of Ni as a function of the s - and d -bandfilling for 1 layer (solid curve), 2 layers (dashed) and 3 layers (dotted).

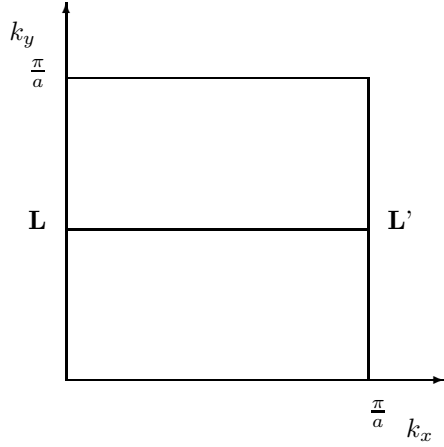


FIG. 8. Irreducible part of the two-dimensional Brillouin zone of Fe for the tight-binding scheme. a is the lattice constant of the monolayer. The main contribution to E_{anis} at $n = 8.8$ (corresponding to $n_d = 7.6$ in the tight-binding calculation) results from the lifting of degeneracies along the line LL' .

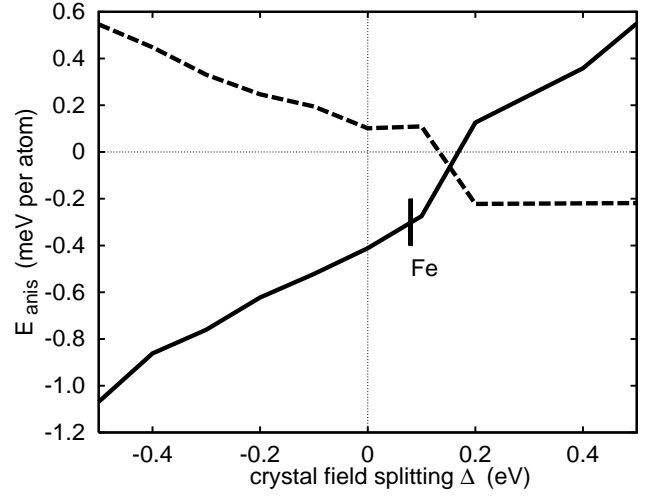


FIG. 9. Dependence of the magnetocrystalline anisotropy energy E_{anis} on the crystal field splitting Δ for the Fe monolayer on Cu(001), $n = 8$, (solid curve) and the Ni monolayer on Cu(001), $n = 10$, (dashed curve). Negative values of E_{anis} yield perpendicular anisotropy. The vertical line denotes the best fit for Δ for the Fe monolayer. In the case of Ni, the fit cannot be improved by the introduction of Δ (see text).

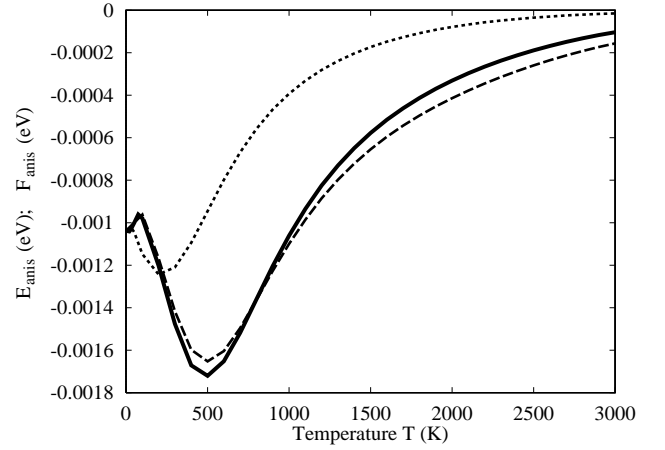


FIG. 10. Temperature dependence of $F_{anis}(T)$ for a Fe-parametrized d -band calculation for the monolayer with d -bandfilling $n_d = 6$. For the dashed curve, only Fermi statistics is taken into account, for the solid curve the lattice expansion is added, and the dotted curve includes the effects of Fermi statistics, lattice expansion and entropy.

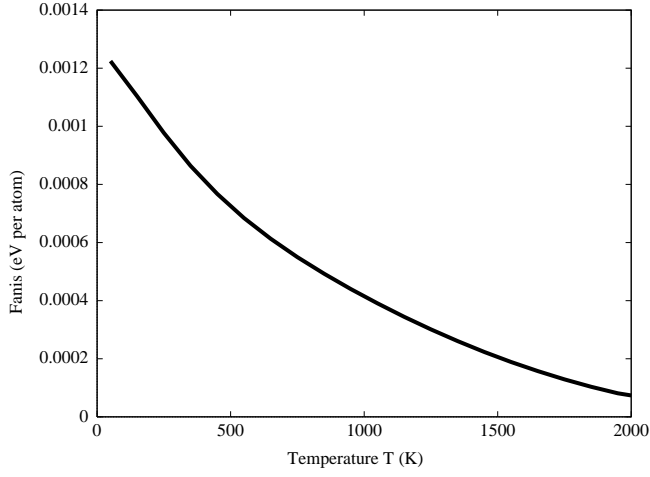


FIG. 11. Temperature dependence of $F_{anis}(T)$ for a Fe-parametrized d -band calculation for 2 layers with d -bandfilling $n_d = 6$. The calculation includes Fermi statistics, lattice expansion and entropy.

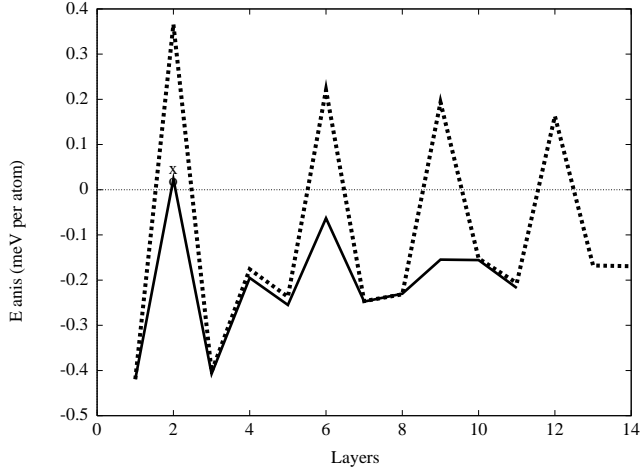


FIG. 12. Magnetic anisotropy energy of Fe as a function of the number of layers calculated in the combined interpolation scheme. The calculation for 1/4 BZ (dashed lines) yields periodic oscillations caused by the incorrect symmetry of $\mathbf{E}_{anis}^{in-plane}$. Summation over 1/2 BZ corrects this problem. • and x are calculations with 15356 and 108228 points in the 1/2 BZ respectively.

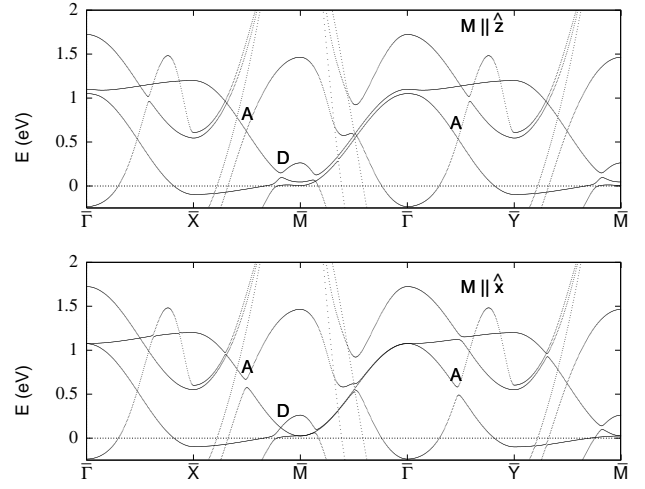


FIG. 13. Monolayer bandstructure of the 3s- and 4s-band for Fe-parameters, calculated within the combined interpolation scheme with the magnetization \mathbf{M} parallel to the layer normal z in the upper part and in-plane parallel x in the lower part. High symmetry points are the same as in Fig. 4.

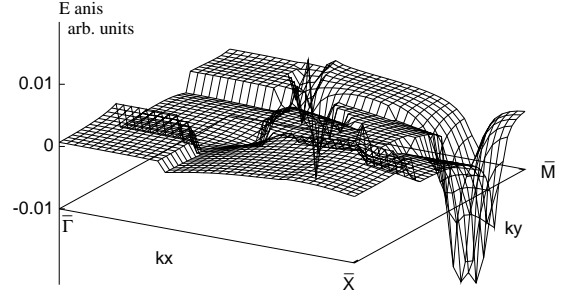


FIG. 14. k -space resolved anisotropy energy for the Fe monolayer at a 3s- and 4d-bandfilling of 7.8. The ring-shaped dip near the M-point is caused by degeneracy D.

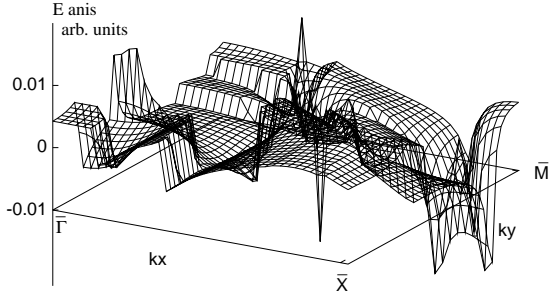


FIG. 15. k -space resolved anisotropy energy of Fe for 3 layers at a $3s$ - and $4d$ -bandfilling of 8.0. The negative peak near the M -point is caused by degeneracy D .

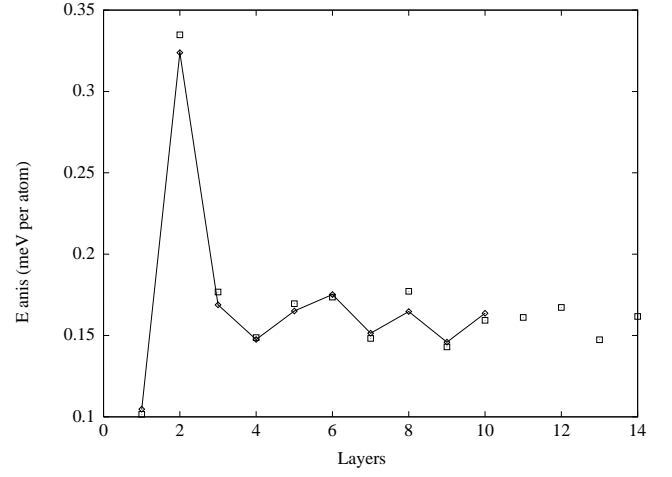


FIG. 17. Magnetic anisotropy energy of Ni as a function of the number of layers, calculated within the combined interpolation scheme. \square is a calculation for $1/4$ BZ with 1722 points, the solid curve is a calculation for $1/2$ BZ with 6188 points.

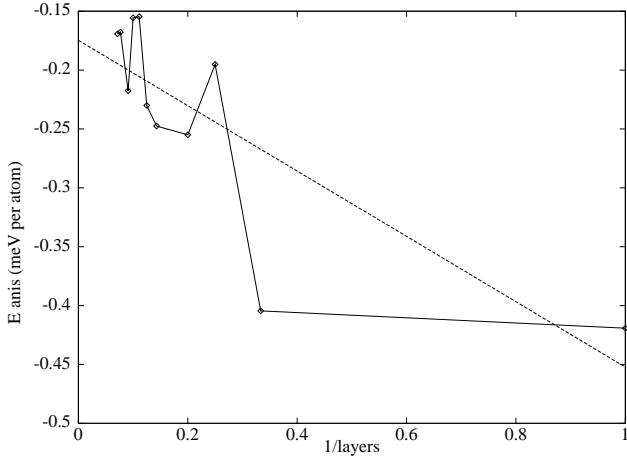


FIG. 16. Magnetic anisotropy energy of Fe as a function of the $1/l$ (l : number of layers). Including the dipole-dipole anisotropy energy, we obtain in-plane magnetization from the fourth layer on. Linear least square fit yields $\mathbf{K}_v = -0.17$ meV per atom and $\mathbf{K}_s = -0.28$ meV per atom.

